Class IIa HDACs inhibit cell death pathways and protect muscle integrity in response to lipotoxicity

Running title: Skeletal muscle lipotoxicity and cell death pathways

Sheree D. Martin[1*], Timothy Connor[1*], Andrew Sanigorski[1], Kevin A. McEwen[1], Darren C. Henstridge[2,3], Brunda Nijagal[4], David De Souza[4], Dedreia L. Tull[4], Peter J. Meikle[3], Greg M. Kowalski[1,5], Clinton R. Bruce[5], Paul Gregorevic[6], Mark A. Febbraio[7], Fiona M. Collier[8], Ken R. Walder[1], Sean L. McGee[1]

[1]Institute for Mental and Physical Heath and Clinical Translation (IMPACT) and Metabolic Research Unit, School of Medicine, Deakin University, Geelong, Victoria 3216, Australia;
[2]College of Health and Medicine, School of Health Sciences, University of Tasmania, Launceston, Australia;
[3]Baker Heart and Diabetes Institute, Melbourne, Victoria 3004, Australia;
[4]Metabolomics Australia, The University of Melbourne, Parkville, Victoria 3010, Australia;
[5]Institute of Physical Activity and Nutrition (IPAN) and School of Exercise and Nutrition Sciences, Deakin University, Geelong, Victoria 3216, Australia;
[6]Centre for Muscle Research, Department of Anatomy and Physiology, The University of Melbourne, Parkville, VIC, Australia.
[7]Monash Institute of Pharmaceutical Sciences, Monash University, Parkville, VIC, Australia.
[8]Barwon Health, Geelong, Victoria 3220, Australia
[*]These authors contributed equally to this work

Lead contact:

Professor Sean L. McGee
Metabolic Remodelling Laboratory
Metabolic Research Unit
School of Medicine
Deakin University, Waurn Ponds, Australia, 3216
Ph: +61 3 5227 2519
Fax: +61 3 5227 2945
Email: sean.mcgee@deakin.edu.au

ABSTRACT

Lipotoxicity, the accumulation of lipids in non-adipose tissues, alters the metabolic transcriptome and mitochondrial metabolism in skeletal muscle. The mechanisms involved remain poorly understood. Here we show that lipotoxicity increased histone deacetylase 4 (HDAC4) and histone deacetylase 5 (HDAC5), which reduced the expression of metabolic genes and oxidative metabolism in skeletal muscle, resulting in increased non-oxidative glucose metabolism. This metabolic reprogramming was also associated with impaired apoptosis and ferroptosis responses, and preserved muscle cell viability in response to lipotoxicity. Mechanistically, increased HDAC4 and 5 decreased acetylation of p53 at K120, a modification required for transcriptional activation of apoptosis. Redox drivers of ferroptosis derived from oxidative metabolism were also reduced. The relevance of this pathway was demonstrated by overexpression of loss-of-function HDAC4 and HDAC5 mutants in skeletal muscle of obese *db/db* mice, which enhanced oxidative metabolic capacity, increased apoptosis and ferroptosis and reduced muscle mass. This study identifies HDAC4 and HDAC5 as repressors of skeletal muscle oxidative metabolism, which is linked to inhibition of cell death pathways and preservation of muscle integrity in response to lipotoxicity.

63 **INTRODUCTION**

64

65 Obesity is driving an epidemic of chronic disease, including type 2 diabetes. Linked to these
66 diseases are adverse cellular responses arising from the accumulation of lipids in non-
67 adipose tissues, a process termed lipotoxicity[1]. The deleterious effects of lipotoxicity include
68 altered cellular signalling, metabolic reprogramming and cell death[2].

69

70 Lipotoxicity alters skeletal muscle metabolism, inducing insulin resistance and impairments
71 in aspects of oxidative metabolism. Reduced rates of both glucose and lipid oxidation have
72 been observed in the skeletal muscle of obese subjects[3, 4] and data describing impairments
73 in amino acid metabolism are also emerging[5, 6, 7]. Experimental induction of acute
74 lipotoxicity in humans through lipid infusion results in many of the same skeletal muscle
75 metabolic alterations[8, 9]. These impairments in oxidative metabolism are associated with
76 reduced expression of a metabolic and mitochondrial transcriptional program controlled by
77 the peroxisome proliferator-activated receptor-gamma coactivator 1 alpha (PGC-1α)
78 transcriptional coactivator[10], encoded by the *PPARGC1A gene*. It is not known why
79 repression of the metabolic transcriptome and reduced oxidative metabolism is an
80 adaptation to lipotoxicity and the molecular pathways involved remain unclear.

81

82 Studies from our group and others have found that the class IIa histone deacetylase (HDAC)
83 isoforms 4 and 5 are regulators of PGC-1α expression in skeletal muscle[11, 12]. HDAC4 and 5
84 act co-operatively as heterodimers to repress the myocyte-enhancer factor 2 (MEF2) family
85 of transcription factors[13, 14]. Binding sites for the MEF2 transcription factor are found in the
86 *PPARGC1A* promoter[12] and in the promoters and enhancer regions of other genes involved

87 in oxidative metabolism[11]. However, the role of the class IIa HDAC transcriptional repressors
88 in the context of lipotoxicity is unknown. We hypothesised that HDAC4 and 5 are increased
89 in response to lipotoxicity and contribute to the suppression of metabolic genes and
90 oxidative metabolism and sought to understand why these adaptations occur.
91

92 **MATERIALS AND METHODS**

93 **Cell culture**

94 Mouse C2C12 myoblasts and myotubes were cultured using standard methods. Cells stably
95 overexpressing HDAC4 and 5 were analysed as myoblasts as HDAC4 and 5 prevented
96 myogenic differentiation of these cells to myotubes. Treatment doses of palmitate,
97 camptothecin, Erastin, 1S,3R-RSL 3 (Merck, Melbourne, Australia) and Ferrostatin
98 (Selleckchem, Houston, Tx, USA) are reported in Figure legends and were applied for 24h
99 unless otherwise stated. Palmitate was dissolved in ethanol at 70°C and diluted in ultrapure
100 H_2O before conjugation to fatty acid-free BSA at 1:10 ratio (w/v). An ethanol/BSA solution
101 without palmitate was prepared at the same time for use as a vehicle.

102

103 **Animal models**

104 All animal experimentation was approved by the Deakin University Animal Ethics Committee
105 (G27-2012 and G21-2015). Mice were acquired from the Animal Resources Centre (Perth,
106 Australia) and were group housed with a 12hr light/dark cycle, temperature 21± 3°C,
107 humidity 30-70% with *ad libitum* access to standard rodent chow and water. Heterozygous
108 *db/+* and homozygous *db/db* mice on a C57BL/6J background were fasted for 5 hr prior to
109 humane killing by cervical dislocation for rapid excision of tissues, which were snap frozen in
110 liquid nitrogen. C57BL/6J mice were administered recombinant serotype 6 adeno-associated
111 viral (AAV6) (rAAV6) vectors via intramuscular injection into the anterior and posterior
112 compartments of the lower hind limbs. Each compartment of the left limb received $2e^{10}$
113 vector genomes (vg) of empty rAAV6, whilst each compartment of the right limb received
114 $1e^{10}$ vg of WT HDAC4 rAAV6 and $1e^{10}$ vg of WT HDAC5 rAAV6. *db/db* mice were similarly
115 administered rAAV6 vectors via intramuscular injection. Each compartment of the left limb

116 received $5e^{10}$ vg of empty rAAV6, whilst each compartment of the right limb received $2.5e^{10}$
117 vg of DN HDAC4 rAAV6 and $2.5e^{10}$ vg of DN HDAC5 rAAV6. Experiments were performed ~8
118 weeks after rAAV6 administration. At the conclusion of experiments mice were fasted for 4
119 hours before humane killing by cervical dislocation. Tissues were rapidly excised and snap
120 frozen in liquid nitrogen or fixed in 10% formalin.
121
122 **Respiration and mitochondrial function analysis**
123 Mitochondrial function in cells treated with vehicle (BSA) or palmitate was assessed as
124 previously described[15] and respiratory analysis of skeletal muscle biopsies was also
125 performed as previously described[11].
126
127 **Lipidomics and metabolite analysis**
128 To determine cellular lipid profiles, ~$1e^6$ cells were collected in 100µl of PBS and frozen at -
129 80°C, or ~10mg of muscle was homogenised in 100µl of PBS, and lipids were determined as
130 previously described [16]. For detection of Glu and GSH, cells in 6-well plates underwent
131 metabolic arrest by washing in 1mL ultrapure water before being frozen instantaneously by
132 the addition of liquid nitrogen. To extract polar metabolites, ice-cold methanol:chloroform
133 (9:1) containing internal standards (0.5nM 13C-sorbitol and 5nM 13C, 15N-valine) was
134 added. Metabolites were detected using LC and high resolution QTOF mass spectrometry
135 previously described[17] with the following modifications. Samples (10µL) were injected onto
136 an Agilent 1290 LC fitted with a SeQuant ZIC®-pHILIC column (2.1 x 150 mm, 5µm; Merck)
137 using 20mM ammonium carbonate, pH 9.0 (Sigma-Aldrich) and 100% acetonitrile as the
138 mobile phases.
139

140

141 **Microarray and gene expression analysis**

142 For comparative transcriptomics analysis, each group consisted of three biological replicates
143 and microarray analysis was performed as previously described[11] and conform to MIAME
144 guidelines. Genes found to be significantly altered in the same direction in both cell and
145 skeletal muscle data sets (n = 236) were analysed by gene set enrichment analysis using
146 KEGG pathways. Gene expression was measured using real time RT-PCR as previously
147 described[18]. Primer sequences are available in Table S1.

148

149 **Immunoprecipitation and western blot analysis**

150 Cells were collected in lysis buffer (50mM Tris pH 7.5, 1mM EDTA, 1mM EGTA, 10% glycerol,
151 1% Triton X-100, 50mM NaF, 5mM sodium pyrophosphate, 1mM DTT, 1X protease inhibitor
152 cocktail (Merck)) and ~20mg skeletal muscle was homogenised in 10 volumes of lysis buffer
153 using a handheld homogeniser. Protein concentration was determined using the BCA assay
154 (Pierce). Immunoprecipitation and western blotting were performed as previously
155 described[19]. Antibody details are listed in Table S2.

156

157 **Insulin/isotopic glucose administration and stable isotope metabolomics**

158 Mice were administered 200uCi/kg of 2[1,2-^{3}H]-deoxyglucose and 100uCi/kg of 1-^{14}C
159 glucose, with or without 1.2U/kg insulin, following a 5hr fast. Blood glucose was determined
160 using a handheld glucometer (Accu-Chek Performa, Merck) and ~5µL blood was obtained
161 from the tail tip prior to tracer administration and 5, 15 and 30min after tracer
162 administration. Plasma tracer concentration and tissue 2-deoxyglucose clearance were
163 determined as we have previously described [20]. To determine 1-^{14}C glucose incorporation

164 into glycogen, ~10-15mg of tibialis anterior muscle was digested in 1M KOH at 70°C for 20
165 min and glycogen was precipitated with saturated Na_2SO_4, washed twice with 95% ethanol
166 and resuspended in acetate buffer (0.84% sodium acetate, 0.46% acetic acid, pH 4.75)
167 containing 0.3mg/mL amyloglucosidase (Merck). Glycogen was digested overnight at 37°C
168 before glucose content was quantified using the glucose oxidase method[15] and ^{14}C-glucose
169 incorporation was measured. To determine 1-^{14}C glucose incorporation into lipids, 5-10mg
170 of TA muscle was homogenised in chloroform/methanol (2:1) and mixed overnight at room
171 temperature. Organic and inorganic phases were separated, and the lower organic phase
172 was collected and evaporated under N_2 at 45°C. The dried extract was resuspended in
173 absolute ethanol and TG content was assayed using TG GPO-PAP reagent (Merck) and ^{14}C-
174 glucose incorporation was measured.
175
176 To assess oxidative glucose utilisation, mice were administered a bolus of 50mg of [U-^{13}C]
177 glucose (Sigma-Aldrich) via oral gavage. At 60 min later, mice were humanely killed by
178 cervical dislocation and skeletal muscles were immediately collected. Targeted
179 metabolomics and analysis of [U-^{13}C] labelling was performed as we have previously
180 described[20].
181
182 **Measurement of apoptosis and cell viability**.
183 Analysis of apoptotic cells was performed by dual staining with FITC-conjugated Annexin V
184 (Merck) and propidium iodide (PI; Thermo-Fischer, Waltham, MA, USA) and was optimised
185 for adherent cells. For measurement of apoptosis in tissues, caspase 3 activity was
186 measured using Caspase-Glo 3/7 assay (Promega, Alexandria, Australia). Quantification of

187 viable cells was performed by staining with 7-aminoactinomycin D (7-AAD; Merck) and flow
188 cytometry or with crystal violet staining with colorimetric detection.

189 **Reactive oxygen species detection**

190 In cells, hydrogen peroxide (H_2O_2) was detected using Amplex Red assay (Invitrogen, Mt
191 Waverly, Australia). Cells were seeded into a 96-well plate at 25,000 cells/well. The
192 following day, cells were treated with vehicle (DMSO), 100µM mitoTEMPO or 100µM
193 apocynin for 30 min at 37°C. Cells were then co-incubated with 50µM Amplex Red and
194 0.1U/ml horseradish peroxidase (HRP) for a further 30 min at 37°C. Mitochondrial ROS was
195 designated as that sensitive to MitoTEMPO, while NADPH oxidase ROS was designated as
196 that sensitive to apocynin. For tissues, the OxiSelect In Vitro ROS/RNS Assay kit (Green
197 Fluorescence) (Cell Biolabs Inc., San Diego, CA, USA) was used according to the
198 manufacturer's instructions.

199

200 **GPX4 activity and lipid peroxidation**

201 Glutathione dependent peroxidase activity was measured using a colorimetric Glutathione
202 Peroxidase Assay Kit (AbCam). Cells were plated into 10cm tissue culture plates at $4x10^6$
203 cells per dish. After 3hrs, media was refreshed and cells incubated for 1hr, washed and
204 collected in 250ul of supplied assay buffer. For tissues, muscle lysate was analysed. Data
205 was then analysed as described by the manufacturer with results normalized to protein
206 concentration. Lipid peroxidation in both cells and muscle lysates was assessed using a lipid
207 peroxidation kit (Sigma). The assay was performed according to manufacturer's instructions,
208 including addition of butanol to the reaction.

209

210 **Histology**

211 Fixed TA muscles were embedded in paraffin before transverse sections were obtained at
212 5μm thickness and stained for H&E and Masson's trichrome. Slides were scanned (Aperio,
213 Leica Biosystems) and were analysed using photoshop and image J.

214 **Statistical analysis.**

215 All data are expressed as mean ± SEM. Individual data points identified as greater than two
216 standard deviations away from the mean were designated as outliers and removed. Data
217 was assessed for normality using the Shapiro-Wilk test. Differences between groups were
218 assessed using t-test, Kruskal-Wallis test, one-way ANOVA or two-way ANOVA as
219 appropriate using GraphPad Prism. Specific differences between groups were identified
220 using Dunn's or Tukey's multiple comparisons tests. For animal experiments where
221 opposing hind limbs were administered different rAAVs, such that control and experimental
222 conditions were contained within the one animal, paired t-tests were used. Differences
223 were considered statistically significant where $p<0.05$.

224

225

226 **RESULTS**

227

228 **HDAC4 and 5 are increased in models of lipotoxicity**

229

230 To test the hypothesis that HDAC4 and 5 are increased by lipotoxicity, C2C12 myotubes
231 were exposed to 0.25 or 0.5mM palmitate, or BSA (vehicle), for 16 hr. Application of 0.5mM
232 palmitate induced alterations consistent with lipotoxicity in muscle cells, including increased
233 ceramide, diglyceride (DG) and triglyceride (TG) levels (Fig. 1A and S1A), lower *Ppargc1a*
234 gene expression (Fig. 1B) and a reduction in cellular respiration (Fig. 1C). The abundance of
235 both HDAC4 and HDAC5 protein was increased by 0.5mM palmitate, while HDAC5 protein
236 abundance was also increased by 0.25mM palmitate (Fig. 1D). There were no differences in
237 *Hdac4* or *Hdac5* gene expression between groups (Fig. S1B).

238

239 To examine whether skeletal muscle HDAC4 and 5 are increased in an *in vivo* model of
240 lipotoxicity, the TA skeletal muscle of obese *db/db* and control heterozygous littermate mice
241 was analysed. Total ceramide and DG were were increased in skeletal muscle of *db/db* mice,
242 while there was a trend for TG to also be higher (Fig. 1E and S1C). Increased muscle lipid
243 concentrations in were associated with decreased *Ppargc-1*α gene expression (Fig. 1F),
244 reduced skeletal muscle respiratory responses (Fig. 1G) and increased HDAC4 and 5 protein
245 abundance (Fig. 1H). Skeletal muscle gene expression levels of *Hdac5*, but not *Hdac4*, were
246 increased in *db/db* mice (Fig. S1D). Notwithstanding the complex physiology of the *db/db*
247 model, these data suggest that skeletal muscle HDAC4 and 5 are increased in response to
248 lipotoxicity and are associated with reduced *Ppargc1a* expression and impaired oxidative
249 metabolism.

250 **Overexpression of HDAC4 and 5 in skeletal muscle represses *Pppargc1a* expression and**
251 **oxidative capacity**
252
253 To examine whether increased HDAC4 and 5 impacts skeletal muscle metabolism, a bilateral
254 skeletal muscle HDAC4 and 5 mouse model was developed using rAAV6 vectors expressing
255 HDAC4 and HDAC5 (Fig. 2A). In TA muscle, this model had increased *Hdac4* and *Hdac5* gene
256 expression (Fig. 2B) and protein (Fig. 2C). Overexpression of HDAC4 and 5 reduced *Ppargc1a*
257 expression (Fig. 2D) and the expression of a range of MEF2 and PGC-1α target genes
258 involved in oxidative and mitochondrial metabolism (Fig. 2E). These changes in metabolic
259 transcripts were associated with reduced protein abundance of ATP synthase subunits, but
260 not other subunits of electron transport chain complexes (Fig. 2F). Reduced ATP synthase
261 components was associated with blunted respiratory responses in muscles overexpressing
262 HDAC4 and 5 when driven by both succinate (Fig. 2G) and malate (Fig. 2H) as substrates.
263 Overexpression of HDAC4 and 5 was not associated with lipid accumulation (Fig. 2I). These
264 data indicate that increasing HDAC4 and 5 represses *Ppargc1a* gene expression and
265 oxidative capacity in skeletal muscle.
266
267 **Overexpression of HDAC4 and 5 in skeletal muscle inhibits oxidative glucose utilisation**
268
269 Reduced skeletal muscle oxidative capacity associated with lipotoxicity is linked with
270 reduced insulin action and impaired glucose utilisation[4, 21, 22]. In bilateral skeletal muscle
271 HDAC4 and 5 mice administered either vehicle or insulin and glucose tracers, glucose
272 clearance was increased in skeletal muscles overexpressing HDAC4 and 5 (Fig. 3B). When
273 expressed relative to control skeletal muscle within each mouse, HDAC4 and 5

274 overexpression increased glucose clearance in vehicle but not insulin-stimulated conditions
275 (Fig. 3C). Insulin reduced the excursion of both glucose tracers (Fig. S2A-B). Overexpression
276 of HDAC4 and 5 increased glucose incorporation into glycogen (Fig. 3D) and increased
277 glycogen concentration (Fig. S2C). In contrast, insulin increased glucose incorporation into
278 lipids (Fig. 3E), which was associated with increased Akt phosphorylation at T308 (Fig. 3G)
279 and S473 (Fig. 3H). Consistent with glucose clearance, phosphorylation of TBC1D4 at S642
280 was increased in skeletal muscle overexpressing HDAC4 and 5 (Fig. 3I).
281
282 This was further explored using a targeted stable isotope metabolomics approach in
283 bilateral skeletal muscle HDAC4 and 5 mice (Fig. 3J). Overexpression of HDAC4 and 5
284 increased the abundance of lactate and succinate (Fig. 3K) and total ^{13}C labelling of
285 succinate and malate (Fig. 3L). Isotopologue analysis revealed accumulation of both M+0
286 and M+2 lactate in muscle overexpressing HDAC4 and 5 (Fig. 3M), suggesting both increased
287 non-oxidative glucose utilisation and increased malate/pyruvate cycle flux, respectively[23].
288 Succinate M+0, M+1 and M+2 isotopologues were increased in muscle overexpressing
289 HDAC4 and 5 (Fig. 3N), consistent with a major impairment in SDH activity[24], which is
290 bifunctional for both the TCA cycle and the electron transport chain. These data are also
291 supported by reduced succinate-driven respiration in muscles overexpressing HDAC4 and 5
292 (Fig. 2G). Similarly, HDAC4 and 5 overexpression was associated with increased malate M+0
293 and M+1 isotopologues (Fig. 3O). Together, these data indicate that increased HDAC4 and 5
294 is linked with defective oxidative glucose utilisation and increased non-oxidative glucose
295 utilisation in skeletal muscle.
296

297 **HDAC4 and 5 enhance cell survival in response to lipotoxicity and supress the apoptosis**
298 **and ferroptosis cell death pathways**
299
300 To better understand why this metabolic reprogramming occurs, important genes regulated
301 by HDAC4 and 5 in the context of lipotoxicity were identified using a comparative
302 transcriptomics approach. Specifically, the transcriptome altered in the skeletal muscle of
303 *db/db* mice in which HDAC4 and 5 was increased (Fig. 1J) was compared to the
304 transcriptome altered in myogenic C2C12 myoblasts stably overexpressing HDAC4 and 5
305 (Fig. S3A). Overexpression of HDAC4 and 5 in these cells reduced *Ppargc1a* gene expression,
306 suppressed OXPHOS and TCA cycle genes, and reduced oxidative capacity (Fig. S3B-D). The
307 comparative transcriptomic analysis and subsequent pathway analysis of coregulated genes
308 revealed the p53 signalling pathway related to cell survival as the only significantly
309 regulated pathway (Fig. S3E).
310
311 Profiling of downstream genes in this pathway in C2C12 myoblasts overexpressing HDAC4
312 and 5 revealed that several pro-apoptosis genes were reduced, including *Casp3* and *9, Cycs,*
313 *Pmaip1* and *Bbc3* (Fig. 4A), consistent with suppression of apoptosis. Similarly, genes
314 involved in ferroptosis, a form of iron-mediated cell death involving lipid peroxidation [25],
315 were altered in ways that indicated suppression of ferroptosis, including increased *Slc7a11*
316 expression and reduced *Sat1* and *Alox15* expression (Fig. 4A). These data suggest that
317 increased HDAC4 and 5 inhibit apoptotic and ferroptotic cell death pathways. Indeed,
318 overexpression of HDAC4 and 5 in C2C12 myoblasts reduced the number of apoptotic cells
319 following exposure to the apoptosis-inducing agent camptothecin (Fig. 4B). Similarly, cell
320 viability was higher in cells overexpressing HDAC4 and 5 following exposure to the

321 ferroptosis-inducing agent RSL3 (Fig. 4C). These data raised the possibility that suppression
322 of the apoptosis and ferroptosis pathways by HDAC4 and 5 enhances cell survival in
323 response to lipotoxicity. To test this hypothesis, cells were exposed to increasing
324 concentrations of palmitate intended to challenge cell viability. Overexpression of HDAC4
325 and 5 enhanced the viability of cells exposed to both 1 and 2mM of palmitate compared
326 with control cells and resulted in cells being largely resistant to lipotoxicity (Fig. 4D). This
327 protection of cell viability was associated with reduced cleavage of caspase 3 and 9, the
328 irreversible events that trigger apoptosis (Fig. 4E), as well as fewer apoptotic cells (Fig. 4F) in
329 response to increasing concentrations of palmitate. Overexposure of western blots showed
330 that endogenous HDAC4 and 5 were increased by these high concentrations of palmitate
331 (Fig. S3F), similar to the lower concentrations of palmitate characterised previously (Fig. 1E).
332 Similarly, overexpression of HDAC4 and 5 reduced lipid peroxidation, the trigger for
333 ferroptosis induced-cell death, in response to increasing concentrations of palmitate (Fig.
334 4H). These data indicate that increased HDAC4 and 5 inhibit the apoptosis and ferroptosis
335 cell death pathways and enhance cell viability in response to lipotoxicity.
336
337 **HDAC4 and 5 inhibit apoptosis by reducing p53 K120 acetylation**
338
339 In several cancer cell types, HDAC5 has been linked with reduced acetylation of p53 at K120,
340 which inhibits p53 transcriptional activity and the expression of apoptosis genes, which
341 reduces apoptosis sensitivity[26, 27, 28]. Furthermore, acetylation of p53, including at K120, can
342 contribute to the transcriptional regulation of ferroptosis[29]. To explore whether reduced
343 acetylation of p53 at K120 is involved in suppression of apoptosis and ferroptosis by HDAC4
344 and 5 in myogenic cells, C2C12 myoblasts stably overexpressing HDAC4 and 5 were

345 transfected with wild type p53, or p53 in which K120 was mutated to either glutamine
346 (K120Q; acetylation mimetic gain-of function) or arginine (K120R; deacetylation mimetic
347 loss-of-function) (Fig. 5A). The acetylation of p53 at K120 was reduced by the
348 overexpression of HDAC4 and 5 (Fig. 5A). In cells overexpressing HDAC4 and 5, introduction
349 of the $p53^{K120Q}$ acetylation mimetic mutant restored the expression of the pro-apoptosis
350 genes *Casp3, Casp9* and *Cycs* (Fig. 5B). However, the expression of *Slc7a11*, which opposes
351 ferroptosis, was not influenced by expression of this mutant (Fig. 5B). This suggests that
352 reduced acetylation of p53 at K120 by HDAC4 and 5 suppresses apoptosis, but not
353 ferroptosis, transcriptional programs. Expression of $p53^{K120Q}$ also restored apoptosis in
354 HDAC4 and 5 overexpressing cells exposed to the apoptosis-inducing agent camptothecin
355 (Fig. 5C). Although p53 is also known to regulate aspects of cellular metabolism[30], gain and
356 loss-of-function K120 p53 mutants had no effect on either oxidative (Fig. S4A) or glycolytic
357 flux (Fig. S4B). To determine whether p53 K120 acetylation determines cell viability in
358 response to lipotoxicity, cells expressing WT p53 or $p53^{K120R}$ were exposed to 2mM
359 palmitate. However, the $p53^{K120R}$ mutant did not influence cell viability in response to
360 palmitate exposure (Fig. 5D). Furthermore, the apoptosis inhibitor, Z-DED-FMK, had no
361 effect on cell viability in response to palmitate exposure (Fig. 5E), suggesting that other
362 mechanisms are also involved in the cell death response to lipotoxicity.
363
364 **HDAC4 and 5 inhibit multiple metabolic inputs to the ferroptosis pathway**
365
366 The role of ferroptosis-mediated mechanisms of cell death (Fig. 5F) were further explored.
367 The ferroptosis inhibitor Ferrostatin enhanced C2C12 myoblast viability following exposure
368 to 2mM palmitate (Fig. 5G). Overexpression of HDAC4 and 5 enhanced cell viability in

369 response to increasing concentrations of Erastin (Fig. 5H), an agent that induces ferroptosis
370 by inhibiting system x_c and glutamate and cysteine exchange[31], which in turn reduces
371 glutathione (GSH) levels and results in lipid peroxidation through multiple mechanisms (Fig.
372 5F). Consistent with HDAC4 and 5 increasing the expression of *Slc7a11* (Fig. 4A),
373 overexpression of HDAC4 and 5 reduced intracellular glutamate concentrations, tended to
374 increase intracellular GSH and increased the GSH/glutamate ratio (Fig. 5I). This was
375 associated with increased glutathione peroxidase (GPX) activity in cells overexpressing
376 HDAC4 and 5 (Fig. 5J) and reduced total H_2O_2 production (Fig. S4C), including from
377 mitochondria and NADPH oxidases (Fig. 5K). There were no differences in the levels of
378 phosphatidylcholine (PC), lysophosphatidylcholine (LPC), lysophosphatidyl-ethanolamine
379 (LPE) and phosphatidylethanolamine (PE) lipids that undergo peroxidation during
380 ferroptosis[32] in skeletal muscle of bilateral HDAC4 and 5 mice (Fig. S4D). Therefore, these
381 data indicate that increased HDAC4 and 5 alters redox inputs to ferroptosis that are
382 regulated by oxidative capacity.
383
384 **HDAC4 and 5 are required to suppress apoptosis and ferroptosis and maintain muscle**
385 **mass in obese mice**
386
387 To establish whether HDAC4 and 5 suppress apoptosis and ferroptosis in skeletal muscle in
388 response to lipoxicity *in vivo*, a bilateral skeletal muscle loss-of-function HDAC4 and 5 model
389 was developed in obese *db/db* mice using AAV6 vectors (Fig. 6A). This loss-of-function
390 approach employed active-site HDAC4 and 5 mutants (D832N HDAC4 and D861N HDAC5),
391 which we have previously described as acting in a dominant negative (DN) manner when
392 overexpressed[11]. Overexpression of these mutants in skeletal muscle increases the

393 expression of *Ppargc1a* and other metabolic genes and enhance oxidative metabolism[11].
394 Expression of DN HDAC4 and 5 to *db/db* mice increased HDAC4 and 5 gene (Fig. 6B) and
395 protein (Fig. 6C) expression and increased the expression of *Ppargc1a* (Fig. 6D). Consistent
396 with these findings, respiratory responses were increased in muscle expressing DN HDAC4
397 and 5 (Fig. 6E). Expression of DN HDAC4 and 5 increased caspase 3 activity (Fig. 6F) and lipid
398 peroxidation (Fig. 6G), functional readouts of apoptosis and ferroptosis, respectively.
399 Examination of the mechanisms involved in HDAC4 and 5-mediated apoptosis revealed that
400 p53 acetylation of K120 tended to be higher (Fig. 6H), and the expression of p53-dependent
401 pro-apoptosis genes, including *Casp3, Casp9* and *Bbc3* was increased (Fig. 6I). The
402 ferroptosis mechanisms regulated by HDAC4 and 5 were also examined. In contrast to
403 observations in myogenic cells, the expression of *Slc7a11* in skeletal muscle was low and
404 close to assay detection limits (Fig. S5A). This suggests that system x_c likely has only a minor
405 role in the regulation of ferroptosis in skeletal muscle. There were no differences in GPX
406 activity between groups (Fig. S5B). However, expression of DN HDAC4 and 5 increased ROS
407 (Fig. 6J) and increased *Sat1* and *Alox15* expression (Fig. 6K), indicating that increased
408 capacity for lipid peroxidation. Increased apoptosis and ferroptosis in skeletal muscles
409 expressing DN HDAC4 and 5 was associated with reduced mass of the gastrocnemius and
410 the TA muscles (Fig. 6L). In the TA muscle, there was no difference in fibre diameter
411 between groups (Fig. S5C). However, Masson's trichrome staining showed sporadic areas of
412 localised fibrosis in response to DN HDAC4 and 5 overexpression (Fig. 6M). In skeletal
413 muscles overexpressing DN HDAC4 and 5 there were also discreet regions of fibres with
414 centralised nuclei (Fig. 6N), indicative of regenerating muscle fibres. These data show that
415 HDAC4 and 5 are required to suppress apoptosis and ferroptosis and to maintain muscle
416 mass and integrity in obese mice.

421 **DISCUSSION**

422

423 Lipotoxicity has a major impact on the metabolism, function and survival of various tissues
424 including skeletal muscle. The current study has revealed that increases in HDAC4 and 5 in
425 response to lipotoxicity induce transcriptional repression of oxidative metabolism and of the
426 apoptosis and ferroptosis cell death pathways in both myogenic cells and skeletal muscle.
427 The impairment in oxidative metabolism also reduces redox inputs to the ferroptosis
428 pathway. These data indicate that metabolic reprogramming in skeletal muscle in response
429 to lipotoxicity is directly linked with cell survival responses.

430

431 Previous findings revealed that lipotoxicity is associated with suppression of a pro-apoptosis
432 transcriptional program in skeletal muscle, with consequences for maintenance of muscle
433 mass[33]. Our data show that the class IIa HDACs are essential for this response, as loss of
434 HDAC4 and 5 function in skeletal muscle in a model of lipotoxicity increased apoptosis genes
435 and markers of apoptosis, which was associated with reduced muscle mass. Furthermore, a
436 readout of ferroptosis was also increased. The exact contribution of these cell death
437 pathways to the reduction in muscle mass observed remains to be determined. However,
438 inhibition of ferroptosis alone enhanced cell viability following palmitate exposure while
439 inhibition of apoptosis alone did not, possibly revealing a greater importance for ferroptosis.
440 The role of ferroptosis in skeletal muscle pathologies is just emerging but has been
441 implicated in the development of sarcopenia, rhabdomyolysis and inflammatory
442 myopathies[34]. Our study also implicates skeletal muscle ferroptosis in sarcopenic obesity.

443

444 While there is much debate in the literature about the relationship between mitochondrial
445 capacity and function and insulin action[35], the reduction in oxidative capacity induced by
446 HDAC4 and 5 did not result in overt insulin resistance. Overexpression of HDAC4 and 5
447 increased basal glucose clearance, with more glucose directed to glycogen synthesis.
448 Oxidative utilisation of glucose was impaired through the TCA cycle, particularly at the level
449 of succinate. The levels of succinate are thought to reflect the redox state of the
450 mitochondrial coenzyme Q pool, with higher concentrations of reduced CoQ ($CoQH_2$)
451 preventing the oxidation of succinate by SDH[36]. Oxidation of succinate by SDH is tightly
452 associated with reverse electron flow to complex I of the electron transport chain and
453 reduced ROS production[37]. Indeed, succinate oxidation-dependent ROS production is critical
454 for pro-inflammatory cytokine production by macrophages[38], adipose tissue
455 thermogenesis[39] and the activity of carotid body oxygen sensing K^+ channels[40]. In the
456 context of the present study, HDAC4 and 5-mediated impairments in succinate oxidation
457 and reduced ROS production likely contribute to inhibition of the ferroptosis pathway and
458 preservation of cell viability in response to lipotoxicity. Additionally, impairments in TCA
459 cycle activity have recently been found to promote cytosolic glutathione synthesis that
460 increases antioxidant capacity[24], which would also inhibit ferroptosis. Together, these data
461 indicate that inhibition of oxidative substrate utilisation is an important adaptation to
462 lipotoxicity.
463
464 In conclusion, this study provides evidence that in response to lipotoxicity the class IIa
465 HDACs unite impairments in skeletal muscle oxidative metabolism with inhibition of the
466 apoptosis and ferroptosis cell death pathways to preserve muscle integrity. These findings
467 provide key new insights into why certain metabolic adaptations occur in response to excess

468 lipids and advance our understanding of the aetiology of metabolic diseases driven by
469 lipotoxicity and excess nutrient availability.
470
471
472

473 **ACKNOWLEDGEMENTS**

474 The authors wish to thank all members of the Metabolic Reprogramming Laboratory for
475 helpful insights and technical advice and are grateful to the technical staff of the Deakin
476 University Animal Services team. The authors also wish to thank Hongwei Qian for AAV
477 production. This work was supported by grants from the National Health and Medical
478 Research Council (NHMRC: APP1027227, APP1030474 and APP1127059) to SLM. PJM, PG
479 and MAF are supported by Fellowships from the NHMRC.

480

481 **AUTHOR CONTRIBUTIONS**

482 Conceptualization, SDM, TC and SLM; Methodology, SDM, TC, DDS, GMK, CRB, PG, FMC,
483 KRW and SLM; Investigation, SDM, TC, AS, KAM, DCH, BN, DDS, GMK, FMC and SLM;
484 Resources, DLT, PJM, CRB, PG, MAF and SLM; Writing – original draft, SDM, TC and SLM;
485 Writing – review and editing, all authors; Funding acquisition, SLM.

486

487 **DECLARATION OF INTERESTS**

488 The authors declare no competing interests related to this article.

489

490 **AVAILABILITY OF DATA AND MATERIALS**

491 The microarray datasets and are available at Gene Expression Omnibus (GSE215185).

492

493 **REFERENCES**

494

495 1. Lee Y, Hirose H, Ohneda M, Johnson JH, McGarry JD, Unger RH. Beta-cell lipotoxicity
496 in the pathogenesis of non-insulin-dependent diabetes mellitus of obese rats:
497 impairment in adipocyte-beta-cell relationships. *Proceedings of the National*
498 *Academy of Sciences of the United States of America* 1994, **91**(23)**:** 10878-10882.

499

500 2. Schaffer JE. Lipotoxicity: when tissues overeat. *Current opinion in lipidology* 2003,
501 **14**(3)**:** 281-287.

502

503 3. Kelley DE, Simoneau JA. Impaired free fatty acid utilization by skeletal muscle in non-
504 insulin-dependent diabetes mellitus. *The Journal of clinical investigation* 1994, **94**(6)**:**
505 2349-2356.

506

507 4. Simoneau JA, Kelley DE. Altered glycolytic and oxidative capacities of skeletal muscle
508 contribute to insulin resistance in NIDDM. *Journal of applied physiology* 1997, **83**(1)**:**
509 166-171.

510

511 5. Baker PR, 2nd, Boyle KE, Koves TR, Ilkayeva OR, Muoio DM, Houmard JA*, et al.*
512 Metabolomic analysis reveals altered skeletal muscle amino acid and fatty acid
513 handling in obese humans. *Obesity (Silver Spring)* 2015, **23**(5)**:** 981-988.

514

515 6. Lerin C, Goldfine AB, Boes T, Liu M, Kasif S, Dreyfuss JM*, et al.* Defects in muscle
516 branched-chain amino acid oxidation contribute to impaired lipid metabolism.
517 *Molecular metabolism* 2016, **5**(10)**:** 926-936.

518

519 7. White PJ, Lapworth AL, An J, Wang L, McGarrah RW, Stevens RD*, et al.* Branched-
520 chain amino acid restriction in Zucker-fatty rats improves muscle insulin sensitivity
521 by enhancing efficiency of fatty acid oxidation and acyl-glycine export. *Molecular*
522 *metabolism* 2016, **5**(7)**:** 538-551.

523

524 8. Dube JJ, Coen PM, DiStefano G, Chacon AC, Helbling NL, Desimone ME*, et al.* Effects
525 of acute lipid overload on skeletal muscle insulin resistance, metabolic flexibility, and
526 mitochondrial performance. *American journal of physiology Endocrinology and*
527 *metabolism* 2014, **307**(12)**:** E1117-1124.

528

529 9. Richardson DK, Kashyap S, Bajaj M, Cusi K, Mandarino SJ, Finlayson J*, et al.* Lipid
530 infusion decreases the expression of nuclear encoded mitochondrial genes and
531 increases the expression of extracellular matrix genes in human skeletal muscle. *The*
532 *Journal of biological chemistry* 2005, **280**(11)**:** 10290-10297.

533

534 10. Sparks LM, Xie H, Koza RA, Mynatt R, Hulver MW, Bray GA*, et al.* A high-fat diet
535 coordinately downregulates genes required for mitochondrial oxidative
536 phosphorylation in skeletal muscle. *Diabetes* 2005, **54**(7)**:** 1926-1933.

537

538 11. Gaur V, Connor T, Sanigorski A, Martin SD, Bruce CR, Henstridge DC*, et al.* Disruption
539 of the Class IIa HDAC Corepressor Complex Increases Energy Expenditure and Lipid
540 Oxidation. *Cell reports* 2016, **16**(11)**:** 2802-2810.

541

542 12. Czubryt MP, McAnally J, Fishman GI, Olson EN. Regulation of peroxisome
543 proliferator-activated receptor gamma coactivator 1 alpha (PGC-1 alpha) and
544 mitochondrial function by MEF2 and HDAC5. *Proceedings of the National Academy*
545 *of Sciences of the United States of America* 2003, **100**(4)**:** 1711-1716.
546
547 13. Backs J, Backs T, Bezprozvannaya S, McKinsey TA, Olson EN. Histone deacetylase 5
548 acquires calcium/calmodulin-dependent kinase II responsiveness by oligomerization
549 with histone deacetylase 4. *Molecular and cellular biology* 2008, **28**(10)**:** 3437-3445.
550
551 14. Lemercier C, Verdel A, Galloo B, Curtet S, Brocard MP, Khochbin S. mHDA1/HDAC5
552 histone deacetylase interacts with and represses MEF2A transcriptional activity. *The*
553 *Journal of biological chemistry* 2000, **275**(20)**:** 15594-15599.
554
555 15. Martin SD, Morrison S, Konstantopoulos N, McGee SL. Mitochondrial dysfunction has
556 divergent, cell type-dependent effects on insulin action. *Molecular metabolism* 2014,
557 **3**(4)**:** 408-418.
558
559 16. Genders AJ, Connor T, Morrison S, Bond ST, Drew BG, Meikle PJ*, et al.* Reducing
560 hepatic PKD activity lowers circulating VLDL cholesterol. *J Endocrinol* 2020, **246**(3)**:**
561 265-276.
562
563 17. Hortle E, Nijagal B, Bauer DC, Jensen LM, Ahn SB, Cockburn IA*, et al*. Adenosine
564 monophosphate deaminase 3 activation shortens erythrocyte half-life and provides
565 malaria resistance in mice. *Blood* 2016, **128**(9)**:** 1290-1301.

566

567 18. McGee SL, Swinton C, Morrison S, Gaur V, Campbell DE, Jorgensen SB*, et al.*
568 Compensatory regulation of HDAC5 in muscle maintains metabolic adaptive
569 responses and metabolism in response to energetic stress. *FASEB journal : official*
570 *publication of the Federation of American Societies for Experimental Biology* 2014,
571 **28**(8)**:** 3384-3395.

572

573 19. McGee SL, Hargreaves M. Exercise and myocyte enhancer factor 2 regulation in
574 human skeletal muscle. *Diabetes* 2004, **53**(5)**:** 1208-1214.

575

576 20. De Jong KA, Hall LG, Renton MC, Connor T, Martin SD, Kowalski GM*, et al.* Loss of
577 protein kinase D activity demonstrates redundancy in cardiac glucose metabolism
578 and preserves cardiac function in obesity. *Molecular metabolism* 2020, **42:** 101105.

579

580 21. Patti ME, Butte AJ, Crunkhorn S, Cusi K, Berria R, Kashyap S*, et al.* Coordinated
581 reduction of genes of oxidative metabolism in humans with insulin resistance and
582 diabetes: Potential role of PGC1 and NRF1. *Proceedings of the National Academy of*
583 *Sciences of the United States of America* 2003, **100**(14)**:** 8466-8471.

584

585 22. Petersen KF, Dufour S, Befroy D, Garcia R, Shulman GI. Impaired mitochondrial
586 activity in the insulin-resistant offspring of patients with type 2 diabetes. *The New*
587 *England journal of medicine* 2004, **350**(7)**:** 664-671.

588

589 23. Zhang W, Guo C, Jiang K, Ying M, Hu X. Quantification of lactate from various
590 metabolic pathways and quantification issues of lactate isotopologues and
591 isotopmers. *Sci Rep* 2017, **7**(1)**:** 8489.
592
593 24. Ryan DG, Yang M, Prag HA, Blanco GR, Nikitopoulou E, Segarra-Mondejar M*, et al.*
594 Disruption of the TCA cycle reveals an ATF4-dependent integration of redox and
595 amino acid metabolism. *Elife* 2021, **10**.
596
597 25. Jiang X, Stockwell BR, Conrad M. Ferroptosis: mechanisms, biology and role in
598 disease. *Nature reviews Molecular cell biology* 2021, **22**(4)**:** 266-282.
599
600 26. Sykes SM, Mellert HS, Holbert MA, Li K, Marmorstein R, Lane WS*, et al.* Acetylation
601 of the p53 DNA-binding domain regulates apoptosis induction. *Molecular cell* 2006,
602 **24**(6)**:** 841-851.
603
604 27. Tang Y, Luo J, Zhang W, Gu W. Tip60-dependent acetylation of p53 modulates the
605 decision between cell-cycle arrest and apoptosis. *Molecular cell* 2006, **24**(6)**:** 827-
606 839.
607
608 28. Sen N, Kumari R, Singh MI, Das S. HDAC5, a key component in temporal regulation of
609 p53-mediated transactivation in response to genotoxic stress. *Molecular cell* 2013,
610 **52**(3)**:** 406-420.
611

612 29. Jiang L, Kon N, Li T, Wang SJ, Su T, Hibshoosh H*, et al.* Ferroptosis as a p53-mediated
613 activity during tumour suppression. *Nature* 2015, **520**(7545)**:** 57-62.
614
615 30. Berkers CR, Maddocks OD, Cheung EC, Mor I, Vousden KH. Metabolic regulation by
616 p53 family members. *Cell metabolism* 2013, **18**(5)**:** 617-633.
617
618 31. Stockwell BR, Friedmann Angeli JP, Bayir H, Bush AI, Conrad M, Dixon SJ*, et al.*
619 Ferroptosis: A Regulated Cell Death Nexus Linking Metabolism, Redox Biology, and
620 Disease. *Cell* 2017, **171**(2)**:** 273-285.
621
622 32. Kagan VE, Mao G, Qu F, Angeli JP, Doll S, Croix CS*, et al.* Oxidized arachidonic and
623 adrenic PEs navigate cells to ferroptosis. *Nature chemical biology* 2017, **13**(1)**:** 81-90.
624
625 33. Turpin SM, Ryall JG, Southgate R, Darby I, Hevener AL, Febbraio MA*, et al.*
626 Examination of 'lipotoxicity' in skeletal muscle of high-fat fed and ob/ob mice. *The*
627 *Journal of physiology* 2009, **587**(Pt 7)**:** 1593-1605.
628
629 34. Wang Y, Zhang Z, Jiao W, Wang Y, Wang X, Zhao Y*, et al.* Ferroptosis and its role in
630 skeletal muscle diseases. *Front Mol Biosci* 2022, **9:** 1051866.
631
632 35. Muoio DM, Neufer PD. Lipid-induced mitochondrial stress and insulin action in
633 muscle. *Cell metabolism* 2012, **15**(5)**:** 595-605.
634

635 36. Murphy MP, Chouchani ET. Why succinate? Physiological regulation by a
636 mitochondrial coenzyme Q sentinel. *Nature chemical biology* 2022, **18**(5)**:** 461-469.
637
638 37. Chance B, Hollunger G. The interaction of energy and electron transfer reactions in
639 mitochondria. I. General properties and nature of the products of succinate-linked
640 reduction of pyridine nucleotide. *The Journal of biological chemistry* 1961, **236:**
641 1534-1543.
642
643 38. Mills EL, Kelly B, Logan A, Costa ASH, Varma M, Bryant CE*, et al.* Succinate
644 Dehydrogenase Supports Metabolic Repurposing of Mitochondria to Drive
645 Inflammatory Macrophages. *Cell* 2016, **167**(2)**:** 457-470 e413.
646
647 39. Mills EL, Pierce KA, Jedrychowski MP, Garrity R, Winther S, Vidoni S*, et al.*
648 Accumulation of succinate controls activation of adipose tissue thermogenesis.
649 *Nature* 2018, **560**(7716)**:** 102-106.
650
651 40. Fernandez-Aguera MC, Gao L, Gonzalez-Rodriguez P, Pintado CO, Arias-Mayenco I,
652 Garcia-Flores P*, et al.* Oxygen Sensing by Arterial Chemoreceptors Depends on
653 Mitochondrial Complex I Signaling. *Cell metabolism* 2015, **22**(5)**:** 825-837.
654
655
656

657 **FIGURE LEGENDS**

658

659 **Figure 1: HDAC4 and 5 are increased in models of lipotoxicity.** (A) Total Cer, DG and TG
660 lipids (One-way ANOVA; Cer $p<0.0001$ (F(2,14)=73.86, ^{f}Tukey's multiple comparisons test
661 $p<0.0077$ vs. 0mM, *Tukey's multiple comparisons test $p<0.0001$ vs. 0mM and vs 0.25mM;
662 DG $p<0.0001$ (F(2,14)=38.50 *Tukey's multiple comparisons test $p<0.0001$ vs. 0mM and vs
663 0.25mM; TG $p<0.0017$ (F(2,14)=10.38 *Tukey's multiple comparisons test $p=0.0333$ vs.
664 0mM); (B) *Ppargc1a* gene expression (One-way ANOVA $p<0.0161$ (F(2,21)=5.054, ^{f}Tukey's
665 multiple comparisons test $p<0.0484$ vs. 0mM *Tukey's multiple comparisons test $p=0.0210$
666 vs. 0mM); (C) Oxygen consumption rate (OCR; One-way ANOVA $p<0.0255$ (F(2,25)=4.262
667 *Tukey's multiple comparisons test $p<0.0001$ vs. 0mM and vs 0.25mM), and; (D) HDAC4 and
668 5 protein in C2C12 myotubes treated with 0mM (BSA vehicle), 0.25mM or 0.5mM palmitate
669 (PA) for 16 hrs (HDAC4, Kruskal-Wallis test, $p=0.049$ (X^2 = 5.591), *Dunn's multiple
670 comparison test $p=0.0380$; HDAC5, One-way ANOVA, $p=0.038$ (F(2,6)=5.903) ^{f}Tukey's
671 multiple comparisons test $p=0.0318$, *Tukey's multiple comparisons test $p=0.0251$). (E) Total
672 Cer, DG and TG lipids (Unpaired t-tests, Cer $p=0.0094$, DG $p=0.0022$, TG $p=0.0616$); (F)
673 *Ppargc1a* gene expression (Unpaired t-test, $p=0.0357$); (G) Basal, substrate and ADP-driven
674 OCR from muscle biopsies (Two-way ANOVA, $^{\varnothing}$genotype $p=0.0493$, $F(1,33)=4.166$), and; (H)
675 HDAC4 and 5 protein in Control and *db/db* mice (Unpaired t-tests, $^{\#}$HDAC4 $p=0.0375$,
676 $^{\#}$HDAC5 $p=0.0308$). Data are mean±SEM, n=3-6 biological replicates per group for cell
677 experiments and 6-8 per group for animal experiments.

678

679

680 **Figure 2: Overexpression of HDAC4 and 5 in skeletal muscle suppresses *Pppargc1a***
681 **expression and oxidative capacity.** (A) The bilateral AAV6 HDAC4 and 5 overexpression
682 mouse model. (B) *Hdac4* and *Hdac5* gene expression (Paired t-test, #*Hdac4* p=0.0246,
683 #*Hdac5* p=0.0305); (C) HDAC4 and 5 protein; (D) *Ppargc1a* gene expression (Paired t-test,
684 p=0.0006); (E) Metabolic gene expression (Paired t-test, #*Ppard* p=0.0055, #*Cpt1b* p=0.0106,
685 #*Pdk4* p=0.0029, #*Cox7a* p=0.0087, #*CytC* p=0.0020, #*Idh1* p=0.0179, #*Fh* p=0.0015, #*Mcad*
686 p=0.0028, #*Hadh* p=0.0029, #*Echs1* p=0.0023); (F) Respiratory chain complex subunit protein
687 (Paired t-test, #Complex V p<0.0001); (G) Basal, succinate and ADP-driven oxygen
688 consumption rate (OCR) from muscle biopsies (Two-way ANOVA, ∅genotype p=0.0247,
689 F(1,43)=5.417); (H) Basal, malate and ADP-driven OCR from muscle biopsies (Two-way
690 ANOVA, ∅genotype p=0.0036, F(1,37)=9.661), and; (I) Ceramide (Cer), diglyceride (DG),
691 triglyceride (TG), phosphatidylethanolamine (PE), lysophosphatidylethanolamine (LPE),
692 phosphatidylcholine (PC), lysophosphatidylcholine (LPC), phosphatidylinositol (PI),
693 lysophosphatidylinositol (LPI), phosphoglycerol (PG) and phosphatidylserine (PS) lipids in
694 Control and HDAC4 and 5 overexpressing skeletal muscle. Data are mean±SEM, n=4-6 per
695 group.
696
697

698 **Figure 3: Overexpression of HDAC4 and 5 in skeletal muscle inhibits oxidative glucose**
699 **utilisation.** (A) Experimental overview of insulin and isotopic glucose tracers in the bilateral
700 AAV6 HDAC4 and 5 overexpression model. (B) Glucose clearance (Two-way ANOVA,
701 $^{\varnothing}$genotype p=0.0328, F(1,27)=5.061); (C) Glucose clearance in muscle overexpressing HDAC4
702 and 5 relative to Control (Paired t-test, $^{\#}$Vehicle p=0.0355); (D) ^{14}C-glucose incorporation
703 into glycogen (Two-way ANOVA, $^{\varnothing}$genotype p=0.0372, F(1,24)=4.864); (E) ^{14}C-glucose
704 incorporation into lipid (Two-way ANOVA, ^Insulin p=0.0009, F(1,21)=14.94); (F)
705 Representative images of insulin signalling components; (G) pT308 Akt (Two-way ANOVA,
706 ^Insulin p=0.0010, F(1,27)=13.75); (H) pS473 Akt (Two-way ANOVA, ^Insulin p<0.0001,
707 F(1,28)=33.13), and; (I) pS642 TBC1D4 (Two-way ANOVA, $^{\varnothing}$genotype p=0.0011,
708 F(1,25)=13.60) in bilateral AAV6 HDAC4 and 5 mice administered insulin and isotopic
709 glucose tracers. (J) Experimental overview of stable isotope metabolomics in the bilateral
710 AAV6 HDAC4 and 5 overexpression model. (K) Total metabolite abundance (Paired t-test,
711 $^{\#}$Lactate p=0.0447, $^{\#}$Succinate p=0.0355); (L) Total ^{13}C labelling of glycolytic and TCA cycle
712 metabolites (Paired t-test, $^{\#}$Succinate p=0.0447, $^{\#}$Malate p=0.0355); (M) Lactate
713 isotopologue (Paired t-test, $^{\#}$M0 p=0.0448, $^{\#}$M2 p=0.0299); (N) Succinate isotopologues
714 (Paired t-test, $^{\#}$M0 p=0.0230, $^{\#}$M1 p=0.0002, $^{\#}$M2 p=0.0005), and; (O) Malate isotopologues
715 (Paired t-test, $^{\#}$M1 p=0.0178) in bilateral AAV6 HDAC4 and 5 mice administered ^{13}C- glucose
716 tracer. (E) Data are mean±SEM, n=5-8 per group.
717
718

719 **Figure 4: HDAC and 5 enhance cell survival in response to lipotoxicity and supress the**
720 **apoptosis and ferroptosis cell death pathways.** (A) Expression of p53-pathway genes
721 involved in pro-apoptosis, anti-apoptosis, intrinsic apoptosis and ferroptosis (Unpaired t-
722 test, #*Casp3* p=0.0451, #*Casp9* p=0.0057, #*Cycs* p=0.0015, #*Pmaip1* p<0.0001, #*Bbc3*
723 p=0.0253, #*Bcl2* p=0.0034, #*Bcl2l1* p=0.0008, #*Slc7a11* p<0.0001, #*Sat1* p<0.0001, #*Alox15*
724 p=0.0001); (B) Apoptotic cells in response to the apoptosis-inducing agent Camptothecin
725 (Two-way ANOVA, genotype p<0.0001 F(1,12)=349.3, treatment p<0.0001 F(2,12)=270.4,
726 interaction p<0.0001 F(2,12)=149.5; #p<0.05 vs Control for same treatment, *p<0.05 vs
727 vehicle by Tukey's multiple comparisons tests); (C) Cell viability in response to the
728 ferroptosis-inducing agent RSL3 (Two-way ANOVA, genotype p<0.0001 F(1,12)=1645,
729 treatment p<0.0001 F(1,12)=36.09, interaction p<0.0090 F(1,12)=9.665; #p<0.05 vs Control
730 for same treatment, *p<0.05 vs 0.25μM RSL by Tukey's multiple comparisons tests); (D) Cell
731 viability in response to palmitate (Two-way ANOVA, genotype p<0.0001 F(1,12)=3374,
732 treatment p<0.0001 F(2,12)=1012, interaction p<0.0001 F(2,12)=684.8; #p<0.05 vs Control
733 for same treatment, *p<0.05 vs vehicle by Tukey's multiple comparisons tests); (E) Full-
734 length (FL) and cleaved (CL) caspase 3 and 9 in response to palmitate; (F) Apoptotic cells in
735 response to palmitate (Two-way ANOVA, genotype p<0.0001 F(1,12)=1468, treatment
736 p=0.0001 F(2,12)=20.35, interaction p<0.0050 F(2,12)=8.498; #p<0.05 vs Control for same
737 treatment, *p<0.05 vs vehicle by Tukey's multiple comparisons tests); (G) Lipid peroxidation
738 in response to palmitate (Two-way ANOVA, genotype p<0.0001 F(1,12)=313.4, treatment
739 p<0.0103 F(2,12)=67.31; #p<0.05 vs Control for same treatment by Tukey's multiple
740 comparisons tests) in Control and HDAC4 and 5 overexpressing C2C12 myoblasts. Data are
741 mean±SEM, n=3-4 biological replicates per group.
742

743 **Figure 5: HDAC4 and 5 inhibit apoptosis by reducing p53 K120 acetylation and reduces**
744 **multiple metabolic inputs to the ferroptosis pathway**. (A) Acetylated p53 at lysine 120
745 (aK120 p53); (B) Expression of caspase 3 (*Casp3;* One-way ANOVA p=0.0040 X^2=0.8408,
746 ^p<0.05 vs Control + WT p53 and HDAC4&5 + K120Q p53 by Tukey's multiple comparisons
747 test), caspase 9 (*Casp9;* One-way ANOVA p=0.0025 X^2=0.8650, ^p<0.05 vs Control + WT p53
748 and HDAC4&5 + K120Q p53 by Tukey's multiple comparisons test), cytochrome c (*Cycs;* One-
749 way ANOVA p=0.0033 X^2=0.8518, ^p<0.05 vs Control + WT p53 by Tukey's multiple
750 comparisons test) and the cystine/glutamate antiporter xCT (*Slc7a11;* One-way ANOVA
751 p<0.0001 X^2=0.9769, ^p<0.05 vs Control + WT p53 by Tukey's multiple comparisons test); (C)
752 Percentage of apoptotic cells following exposure to camptothecin (One-way ANOVA
753 p=0.0014 X^2=0.8875, ^p<0.05 vs Control + WT p53 and HDAC4&5 + K120Q p53 by Tukey's
754 multiple comparisons test); (D) Cell viability 16 hrs after palmitate exposure (Two-way
755 ANOVA, treatment p<0.0001 F(1,12)=50.44, genotype p=0.0361 F(1,12)=5.56; *p<0.05 vs
756 vehicle for same genotype by Tukey's multiple comparisons tests) in C2C12 myoblasts
757 expressing wild type (WT) or K120R (loss-of-function) p53 treated with vehicle or 2mM
758 palmitate for 24 hrs. (E) Cell viability following palmitate exposure and co-incubation with
759 vehicle (DMSO) or increasing concentrations of Z-DEVD-FMK (One-way ANOVA p=0.3282);
760 (F) Schematic showing key regulatory points in the ferroptosis pathway; (G) Cell viability
761 following palmitate exposure and co-incubation with vehicle (DMSO) or increasing
762 concentrations of Ferrostatin (One-way ANOVA p=0.0323 X^2=0.5337, *p<0.05 vs Vehicle by
763 Tukey's multiple comparisons test); (H) Cell viability following exposure to increasing
764 concentrations of Erastin (Two-way ANOVA, genotype p<0.0001 F(1,18)=293.7, treatment
765 p<0.0001 F(2,18)=139.6, interaction p<0.0001 F(2,18)=50.88; $^\#$p<0.05 vs Control for same
766 treatment, *p<0.05 vs Vehicle same genotype by Tukey's multiple comparisons tests); (I)

767 Glutamate (Glu), glutathione (GSH) and the GSH/Glu ratio (Unpaired t-tests, #Glu p=0.0049,

768 #GSH/Glu p=0.0023); (J) Glutathione peroxidase (GPX) activity (Unpaired t-test, p<0.0001),

769 and; (K) H_2O_2 derived from mitochondria (mito), NADPH oxidases (NOX) and other sources

770 (Unpaired t-tests, #Mito p=0.0105, #NAPDH Ox. p<0.0001, #Other p=0.0004) in Control or

771 HDAC4 and 5 overexpressing C2C12 myoblasts. Data are mean±SEM, n=4-10 biological

772 replicates per group.

773

774

775 **Figure 6: HDAC4 and 5 are required to suppress apoptosis and ferroptosis and maintain**
776 **muscle mass in obese mice.** (A) The bilateral AAV6 dominant negative (DN) HDAC4 and 5
777 overexpression *db/db* mouse model. (B) *Hdac4* and *Hdac5* gene expression (Paired t-tests,
778 #*Hdac4* p=0.0003, #*Hdac5* p=0.0002); (C) HDAC4 and 5 protein; (D) *Ppargc1a* gene
779 expression (Paired t-tests, p=0.0191); (E) Basal, substrate and ADP-driven oxygen
780 consumption rate (OCR) from muscle biopsies (Two-way ANOVA, genotype p=0.0482
781 $F(1,42)$=4.141); (F) Caspase 3 activity (Paired t-tests, p=0.0292); (G) Lipid peroxidation
782 (Paired t-tests, p=0.0013); (H) Acetylated p53 at lysine 120 (aK120 p53); (I) Expression of
783 apoptosis genes (Paired t-tests, #*Casp3* p=0.0036, #*Casp9* p=0.0064, #*Bbc3* p=0.0024); (J)
784 Reactive oxygen species (ROS; Paired t-tests, p=0.0292); (K) Expression of ferroptosis genes
785 (Paired t-tests, #*Sat1* p=0.0257, #*Casp9* p=0.0286); (L) Mass of the gastrocnemius (Gastroc.)
786 and tibialis anterior (TA) skeletal muscles (Paired t-tests, #Gastroc. P<0.0001, #TA p=0.0004);
787 (M) Masson's trichrome staining, and; (N) H&E staining of sections of the TA muscle in
788 Control and DN HDAC4 and 5 overexpressing skeletal muscle in *db/db* mice. Arrows indicate
789 fibres with centralised nuclei. Data are mean±SEM, n=6-10 per group.
790

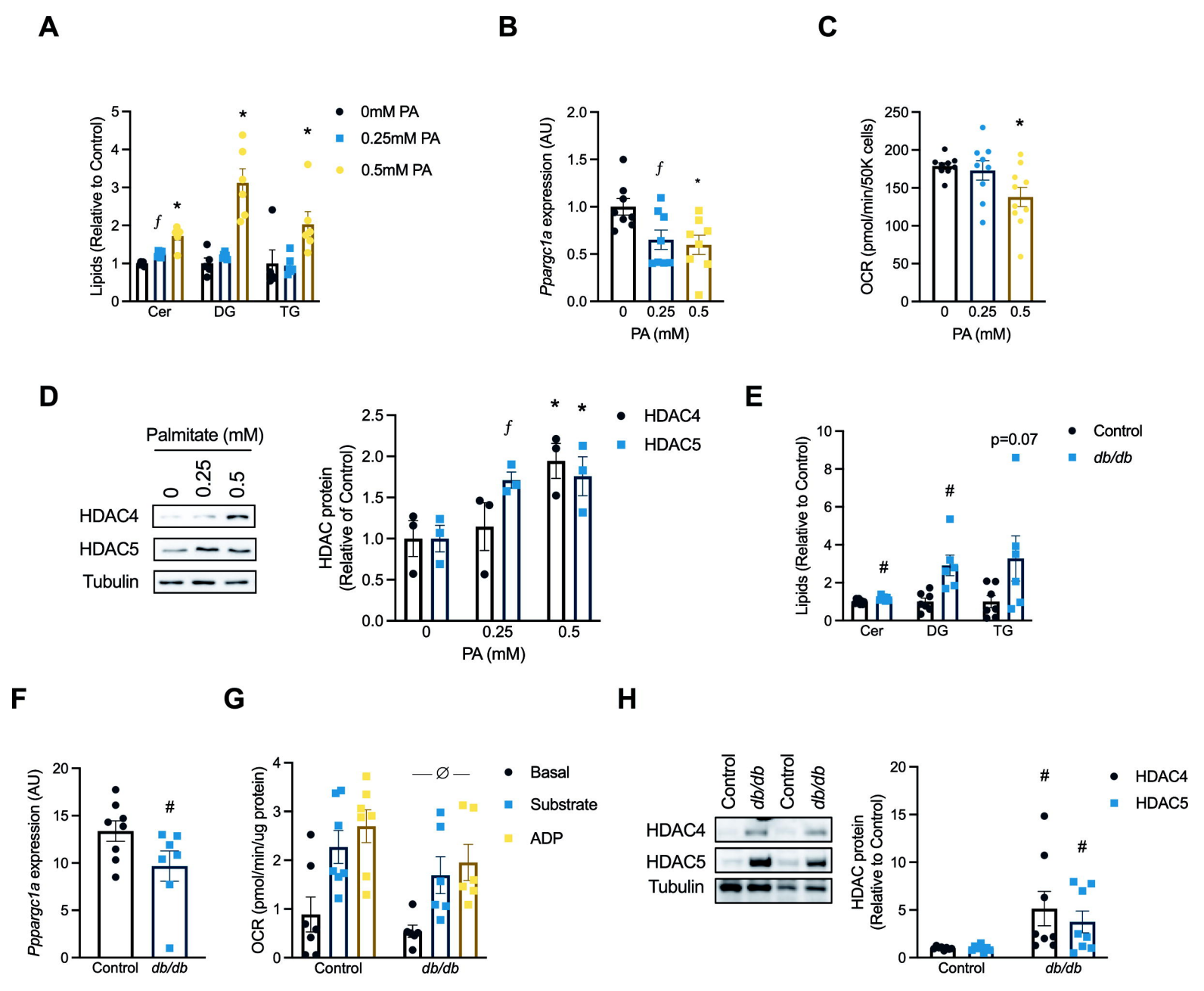
A
Lipids (Relative to Control)
0mM PA
0.25mM PA
0.5mM PA
Cer
DG
TG
B
Ppargc1a expression (AU)
PA (mM)
C
OCR (pmol/min/50K cells)
PA (mM)
D
Palmitate (mM)
0
0.25
0.5
HDAC4
HDAC5
Tubulin
HDAC protein (Relative of Control)
PA (mM)
E
Lipids (Relative to Control)
Control
db/db
p=0.07
Cer
DG
TG
F
Pppargc1a expression (AU)
Control
db/db
G
OCR (pmol/min/ug protein)
Basal
Substrate
ADP
Control
db/db
H
Control
db/db
Control
db/db
HDAC4
HDAC5
Tubulin
HDAC protein (Relative to Control)
HDAC4
HDAC5
Control
db/db

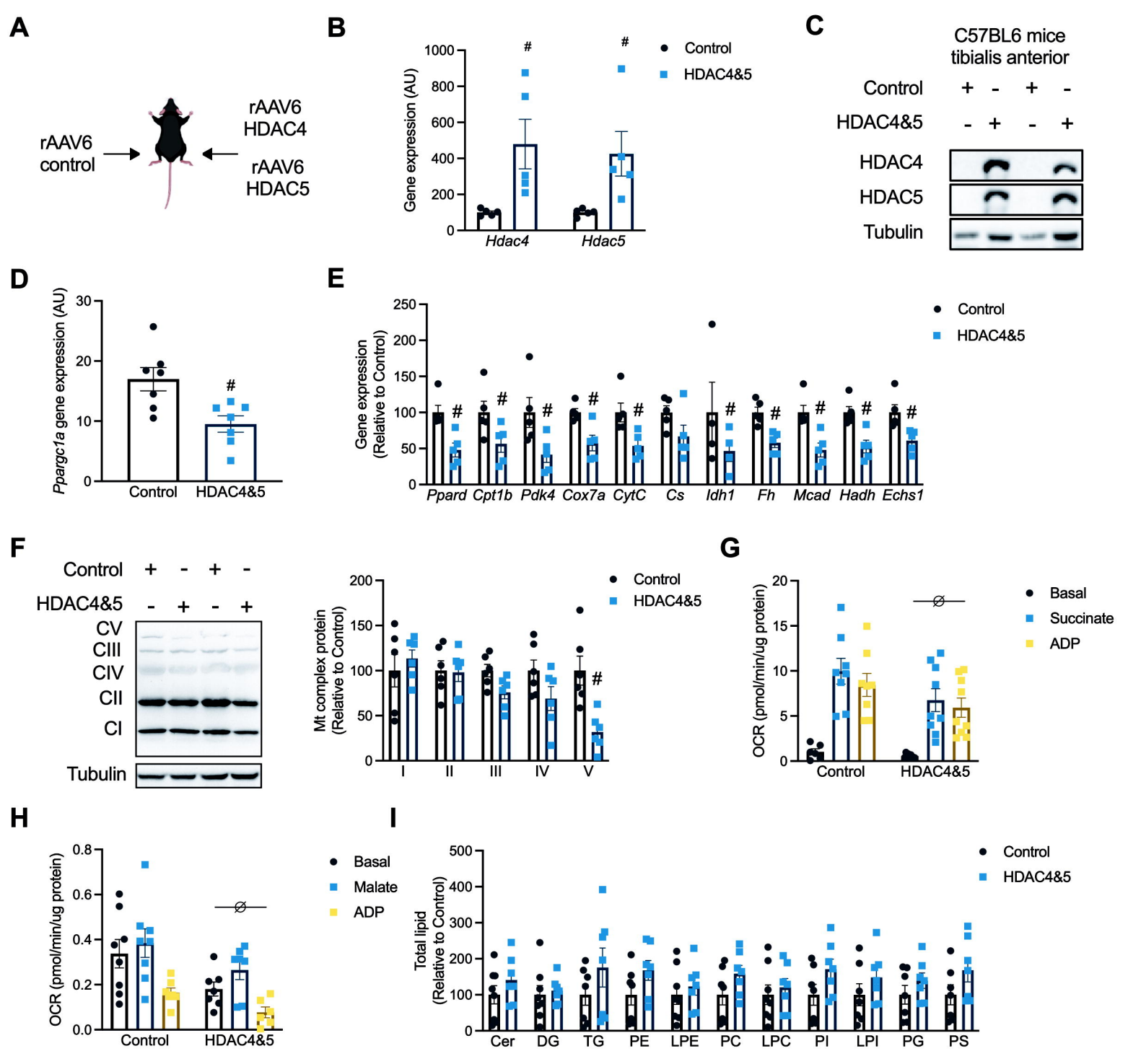
A
rAAV6 control
rAAV6 HDAC4
rAAV6 HDAC5
B
Gene expression (AU)
Control
HDAC4&5
Hdac4
Hdac5
C
C57BL6 mice tibialis anterior
Control
HDAC4&5
HDAC4
HDAC5
Tubulin
D
Ppargc1a gene expression (AU)
Control
HDAC4&5
E
Gene expression (Relative to Control)
Control
HDAC4&5
Ppard
Cpt1b
Pdk4
Cox7a
CytC
Cs
Idh1
Fh
Mcad
Hadh
Echs1
F
Control
HDAC4&5
CV
CIII
CIV
CII
CI
Tubulin
Mt complex protein (Relative to Control)
I
II
III
IV
V
G
OCR (pmol/min/ug protein)
Basal
Succinate
ADP
Control
HDAC4&5
H
OCR (pmol/min/ug protein)
Basal
Malate
ADP
Control
HDAC4&5
I
Total lipid (Relative to Control)
Control
HDAC4&5
Cer
DG
TG
PE
LPE
PC
LPC
PI
LPI
PG
PS

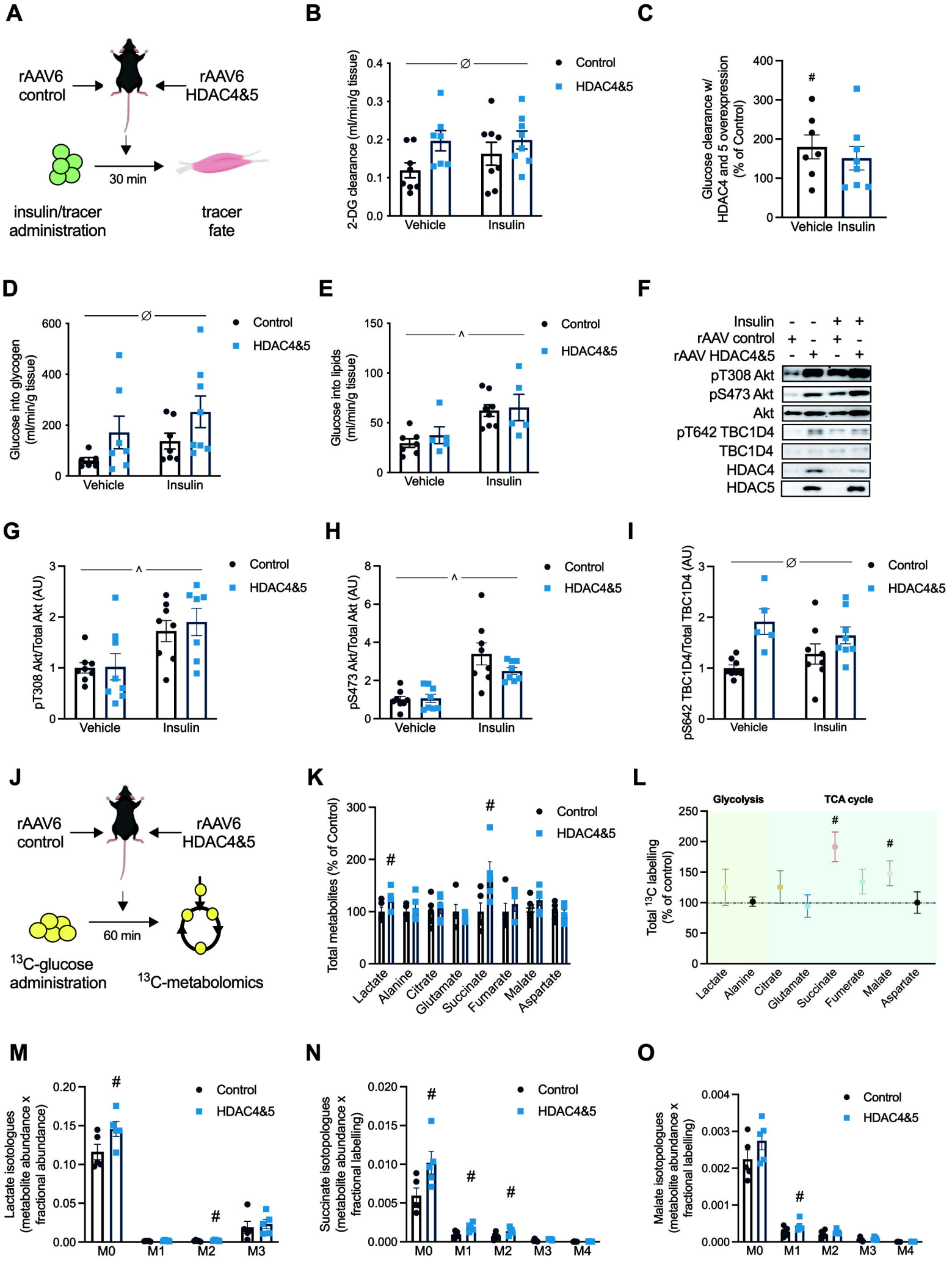
A
rAAV6 control
rAAV6 HDAC4&5
30 min
insulin/tracer administration
tracer fate
B
2-DG clearance (ml/min/g tissue)
Control
HDAC4&5
Vehicle
Insulin
C
Glucose clearance w/ HDAC4 and 5 overexpression (% of Control)
Vehicle
Insulin
D
Glucose into glycogen (ml/min/g tissue)
Control
HDAC4&5
Vehicle
Insulin
E
Glucose into lipids (ml/min/g tissue)
Control
HDAC4&5
Vehicle
Insulin
F
Insulin
rAAV control
rAAV HDAC4&5
pT308 Akt
pS473 Akt
Akt
pT642 TBC1D4
TBC1D4
HDAC4
HDAC5
G
pT308 Akt/Total Akt (AU)
Control
HDAC4&5
Vehicle
Insulin
H
pS473 Akt/Total Akt (AU)
Control
HDAC4&5
Vehicle
Insulin
I
pS642 TBC1D4/Total TBC1D4 (AU)
Control
HDAC4&5
Vehicle
Insulin
J
rAAV6 control
rAAV6 HDAC4&5
60 min
13C-glucose administration
13C-metabolomics
K
Total metabolites (% of Control)
Control
HDAC4&5
Lactate
Alanine
Citrate
Glutamate
Succinate
Fumarate
Malate
Aspartate
L
Glycolysis
TCA cycle
Total 13C labelling (% of control)
Lactate
Alanine
Citrate
Glutamate
Succinate
Fumerate
Malate
Aspartate
M
Lactate isotologues (metabolite abundance x fractional abundance)
Control
HDAC4&5
M0
M1
M2
M3
N
Succinate isotopologues (metabolite abundance x fractional labelling)
Control
HDAC4&5
M0
M1
M2
M3
M4
O
Malate isotopologues (metabolite abundance x fractional labelling)
Control
HDAC4&5
M0
M1
M2
M3
M4

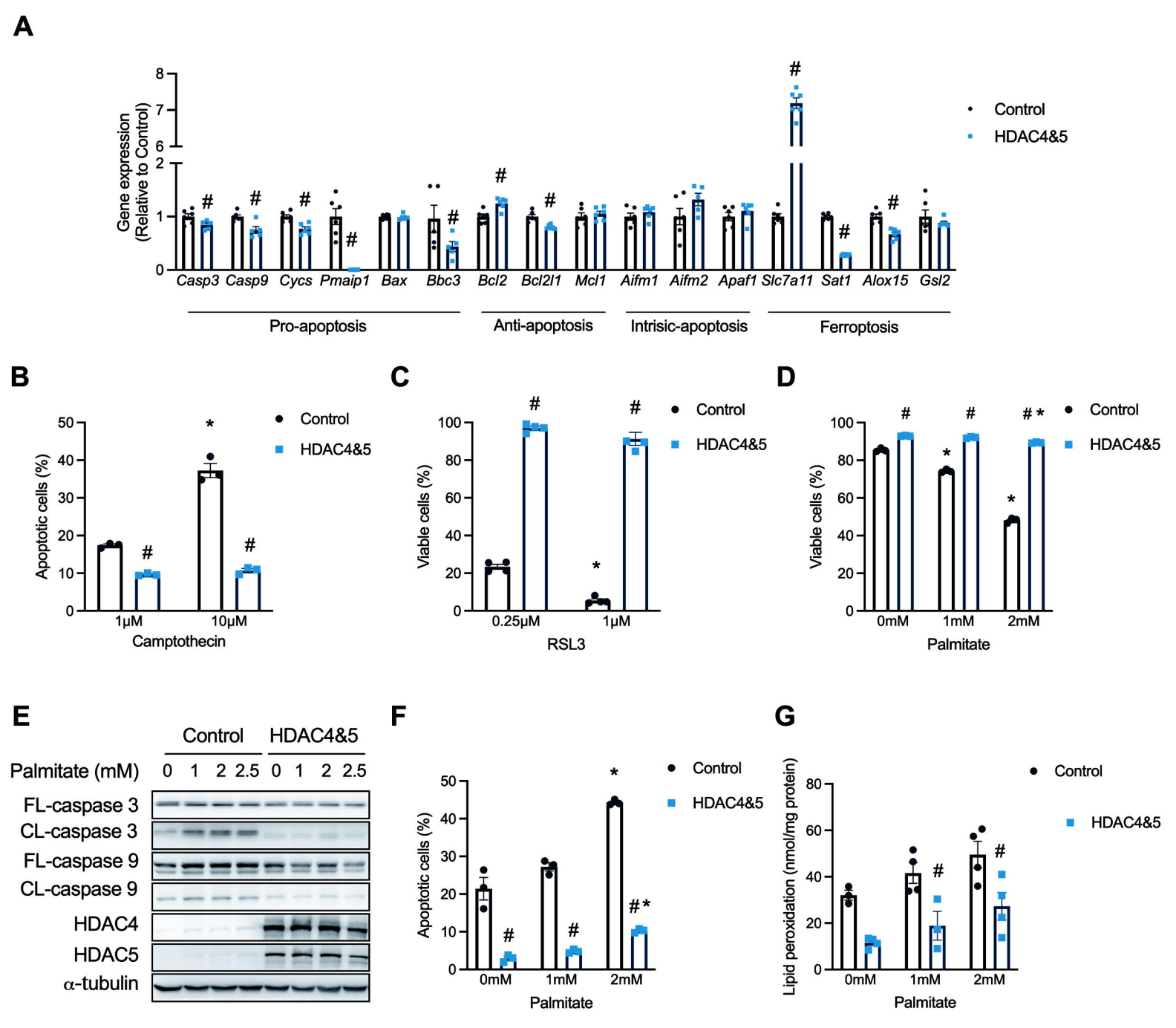
A
Gene expression (Relative to Control)
Control
HDAC4&5
Casp3
Casp9
Cycs
Pmaip1
Bax
Bbc3
Bcl2
Bcl2l1
Mcl1
Aifm1
Aifm2
Apaf1
Slc7a11
Sat1
Alox15
Gsl2
Pro-apoptosis
Anti-apoptosis
Intrisic-apoptosis
Ferroptosis
B
Apoptotic cells (%)
1μM
10μM
Camptothecin
C
Viable cells (%)
0.25μM
1μM
RSL3
D
Viable cells (%)
0mM
1mM
2mM
Palmitate
E
Control
HDAC4&5
Palmitate (mM)
0 1 2 2.5 0 1 2 2.5
FL-caspase 3
CL-caspase 3
FL-caspase 9
CL-caspase 9
HDAC4
HDAC5
α-tubulin
F
Apoptotic cells (%)
0mM
1mM
2mM
Palmitate
G
Lipid peroxidation (nmol/mg protein)
0mM
1mM
2mM
Palmitate

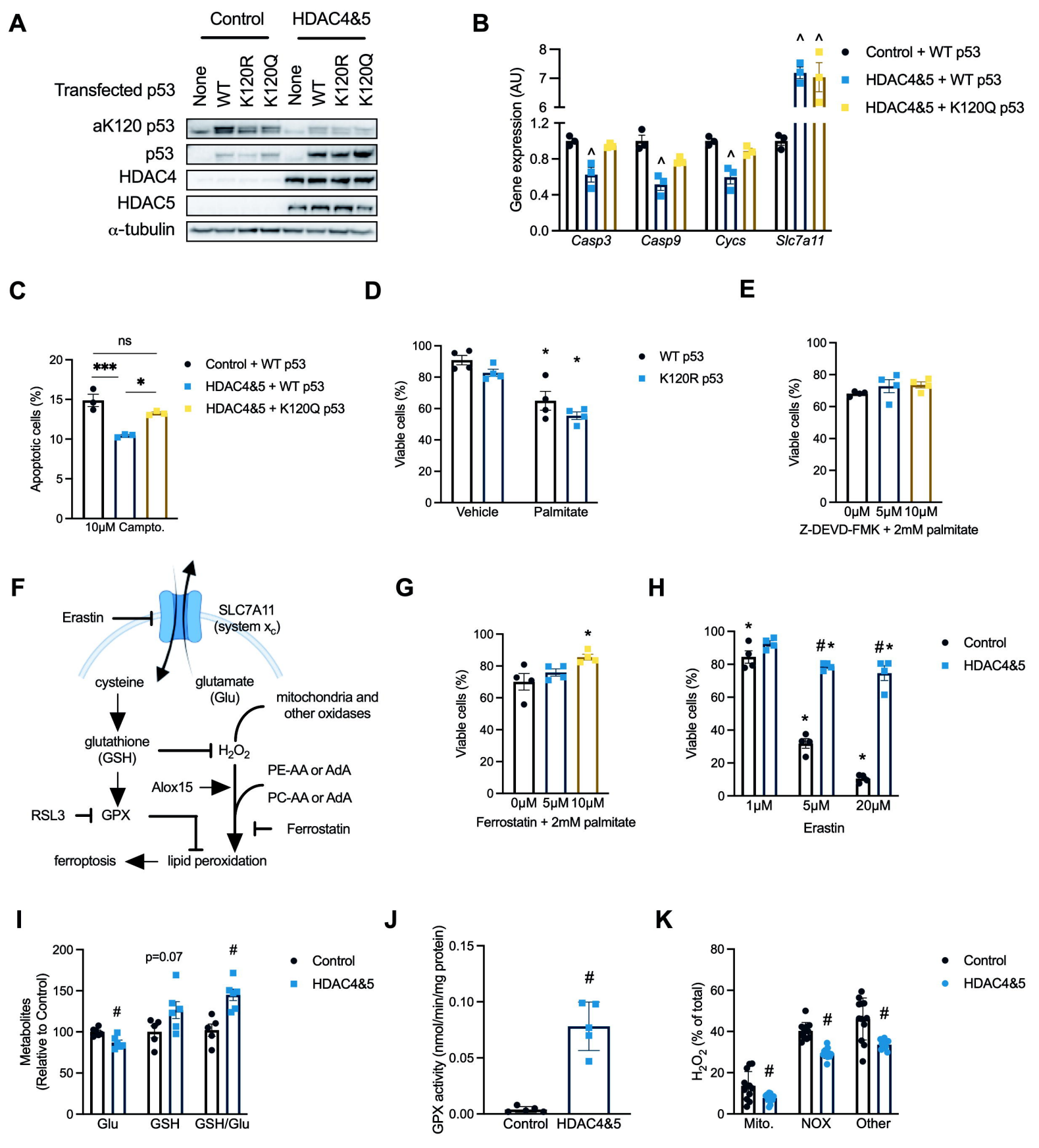
A
Control
HDAC4&5
Transfected p53
None
WT
K120R
K120Q
None
WT
K120R
K120Q
aK120 p53
p53
HDAC4
HDAC5
α-tubulin
B
Gene expression (AU)
Control + WT p53
HDAC4&5 + WT p53
HDAC4&5 + K120Q p53
Casp3
Casp9
Cycs
Slc7a11
C
Apoptotic cells (%)
ns
***
*
10μM Campto.
D
Viable cells (%)
WT p53
K120R p53
Vehicle
Palmitate
E
Viable cells (%)
0μM
5μM
10μM
Z-DEVD-FMK + 2mM palmitate
F
Erastin
SLC7A11
(system x_c)
cysteine
glutamate
(Glu)
mitochondria and
other oxidases
glutathione
(GSH)
H_2O_2
PE-AA or AdA
Alox15
PC-AA or AdA
RSL3
GPX
Ferrostatin
ferroptosis
lipid peroxidation
G
Viable cells (%)
0μM
5μM
10μM
Ferrostatin + 2mM palmitate
H
Viable cells (%)
Control
HDAC4&5
1μM
5μM
20μM
Erastin
I
Metabolites
(Relative to Control)
p=0.07
Control
HDAC4&5
Glu
GSH
GSH/Glu
J
GPX activity (nmol/min/mg protein)
Control
HDAC4&5
K
H_2O_2 (% of total)
Control
HDAC4&5
Mito.
NOX
Other

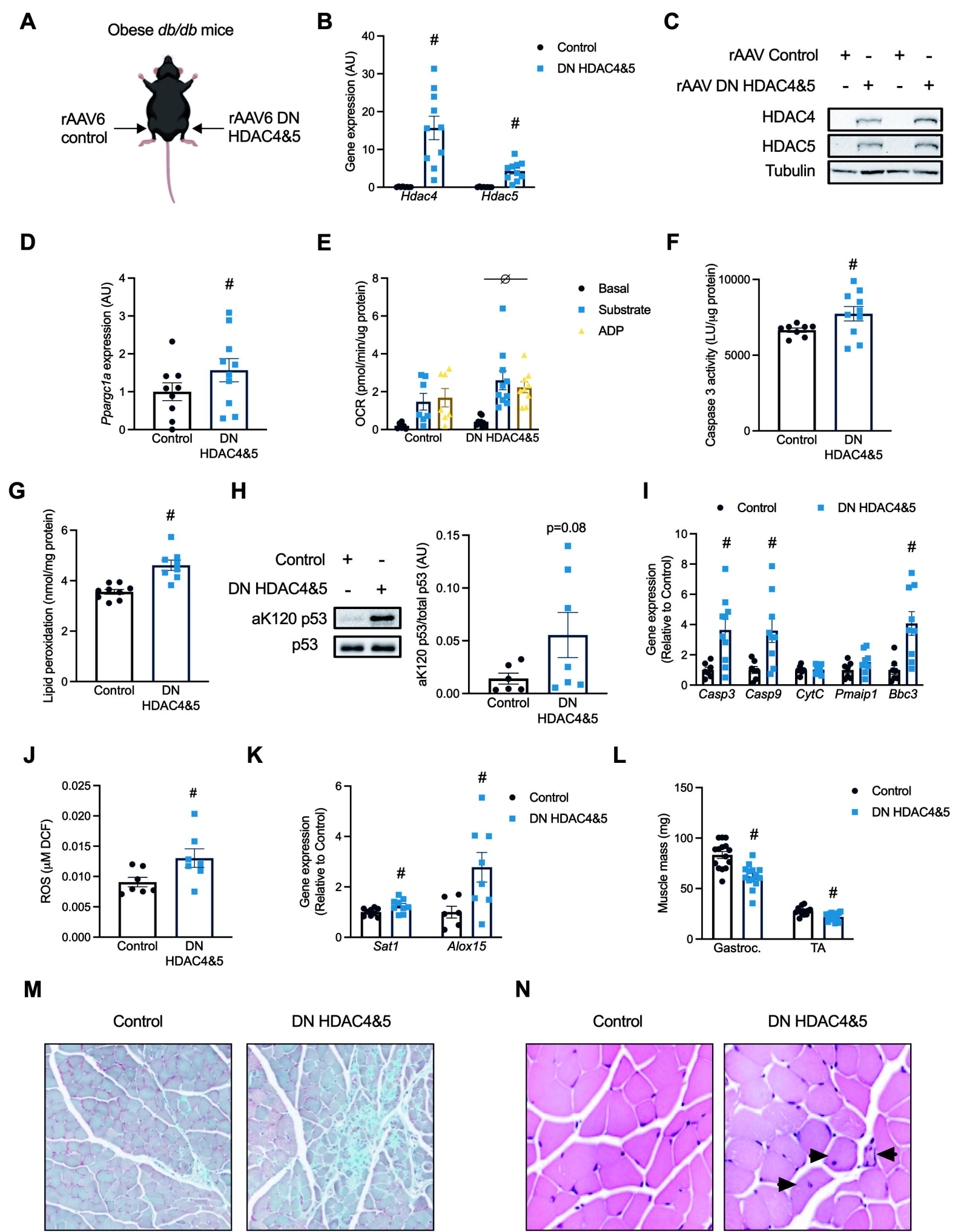
A
Obese db/db mice
rAAV6 control
rAAV6 DN HDAC4&5
B
Gene expression (AU)
Control
DN HDAC4&5
Hdac4
Hdac5
C
rAAV Control
rAAV DN HDAC4&5
HDAC4
HDAC5
Tubulin
D
Ppargc1a expression (AU)
Control
DN HDAC4&5
E
OCR (pmol/min/ug protein)
Basal
Substrate
ADP
F
Caspase 3 activity (LU/µg protein)
G
Lipid peroxidation (nmol/mg protein)
H
aK120 p53
p53
aK120 p53/total p53 (AU)
p=0.08
I
Gene expression (Relative to Control)
Casp3
Casp9
CytC
Pmaip1
Bbc3
J
ROS (µM DCF)
K
Sat1
Alox15
L
Muscle mass (mg)
Gastroc.
TA
M
N